

Nonlinear Temperature Distributions in Bridges at Different Locations in the United States



Izak C. Potgieter
Director
Bruinette Kruger Stoffberg Inc.
Pretoria, South Africa



William L. Gamble
Professor of Civil Engineering
University of Illinois
Urbana, Illinois

As in the case of earthquake loadings or wind loadings which vary significantly throughout the continental United States, a large variation in thermal loadings can be expected. Structures in some parts of the country are more likely to experience large thermal loadings due to specific meteorological conditions. It is not necessary to take the severe conditions experienced in one part of the country into consideration in bridge design for another part of the country where totally different environmental conditions may exist.

The current AASHTO Code¹ deals only marginally with temperature effects in bridge design. The only factors

addressed are overall expansion and contraction and no adjustments are made for variations in weather conditions through the country other than a distinction between "moderate"* and "cold" climates. The two foreign codes that deal extensively with temperature distributions through bridge superstructures are the British BS 5400² and New Zealand Ministry of Works Specifications.³ No variation of design conditions with location are suggested by these two codes, since they are intended as specific design guidelines for the British Isles and New Zealand, respectively. The research on which these

*See AASH TO Specification, Section 3.16.

codes were based indicates that very little variation in thermal loadings occurred with a change in location in the respective countries. Ref. 4 and its derivative Ref. 5 are the first attempts to include a temperature gradient into general American bridge design practice.

The large variations in meteorological conditions in the United States necessitate the quantification of extreme thermal loadings at representative locations throughout the country according to which acceptable design criteria for the American bridge codes can be developed. A heat flow model was developed to analyze the possible influence of weather conditions.

The main emphasis in this paper is the magnitude and effect of nonlinear temperature distributions over the depth of a member. Appendix A contains a brief discussion, with illustrations, of the effects of a particular temperature distribution on a specific rectangular member.

HEAT FLOW COMPUTER MODEL

In order to quantify the magnitude of temperature differences expected in bridge decks at extreme conditions, a one-dimensional computer heat flow model⁶ was used. In the development of the heat flow analysis, extensive use was made of material previously developed. Much of this work had been done in New Zealand and Australia, with work by Priestley et al.,^{7,8} Lanigan et al.,^{9,10} Hunt and Cook,¹¹ Thurston,¹² and Hirst.¹³

The purpose of this study was not the development of new and improved heat flow models but rather the use of these models to study the variability of thermal effects across the continental United States.

The three general processes of heat transfer are conduction, convection and

Synopsis

The effects of nonlinear temperature distributions in bridge structures resulting from solar radiation and other related weather parameters were investigated. A finite difference heat flow model was developed to simulate transient heat flow in bridges. Reasonable agreement was found between computed temperature distributions and experimental measurements for the Kishwaukee River Bridge at Rockford, Illinois.

Meteorological data from 26 SOLMET stations spread across the continental United States were used to compute possible extreme temperature distributions in bridges located at those stations. Temperature differences approaching 57°F (32°C), the value contained in the New Zealand specifications, were obtained for a bare concrete deck located in the desert Southwest United States. Moderate response was found for coastal areas. The temperature difference cited is the differential between the maximum temperature during the day, at the top of the deck, and the minimum temperature, at some section low in the cross section but generally not at the bottom, at the same time.

Simplified relationships of curvature-depth and residual stress-depth due to nonlinear temperature distributions in box girder bridges were developed for application in bridge design at different locations in the United States.

radiation. All three modes are involved in the heat transfer process which takes place in bridges. A finite difference, heat flow model was developed which incorporates the heat transfer variables and weather data for the determination

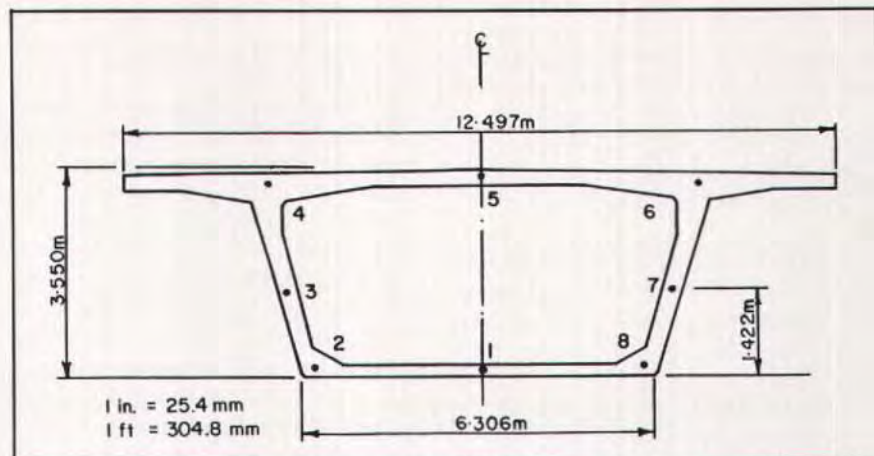


Fig. 1. Cross section of Kishwaukee River Bridge.

of vertical temperature distributions at various times in a typical bridge section.

Two- and three-dimensional heat flow models are also possible, and may be formulated using either finite differences or finite elements. For this study, there seemed to be no advantage to the finite element approach, and the finite difference approach was simpler to implement. Ref. 14 describes a study which used a two-dimensional heat flow model in a study of concrete box girder bridges. This was necessary in Ref. 14 because part of the interest was the temperature gradients through the web thicknesses and in the effects of the orientation of the bridge relative to a north-south axis. Many details were necessary for these purposes.

The one-dimensional heat flow analysis was adequate for this study because the interest was in overall response of bridge structures to a relatively large number of different climatic conditions.

FIELD MEASUREMENTS ON THE KISHWAUKEE RIVER BRIDGE

In order to verify the ability of the

analytical model to predict the temperature distribution in a bridge deck at various times, given the transient weather conditions, field measurements were performed on the Kishwaukee River Bridge.^{15,16} This is a five span segmentally constructed box girder bridge near Rockford, Illinois. It has end spans of 170 ft (51.8 m) and three interior spans of 250 ft (76.2 m) with an overall depth of 11 ft 7 $\frac{3}{4}$ in. (3.55 m). Fig. 1 shows the cross section of the bridge.

Eight Carlson strain gauges were cast into the bridge at each of three different sections of the bridge. In the webs of each of those sections a gauge was located near the top, 4 ft 8 in. (1.4 m) above the soffit and just above the soffit. Strain gauges were also placed above and below the cavity of the box girder section. The deck was paved with 1.75 in. (45 mm) of blacktop. Apart from strain readings for which those gauges were originally intended, temperature readings can also be made. Temperature readings as well as measurements of the related weather parameters were taken for a 56 hour period between July 8 and 10, 1982.

The measurements were compared with the results of the computer heat

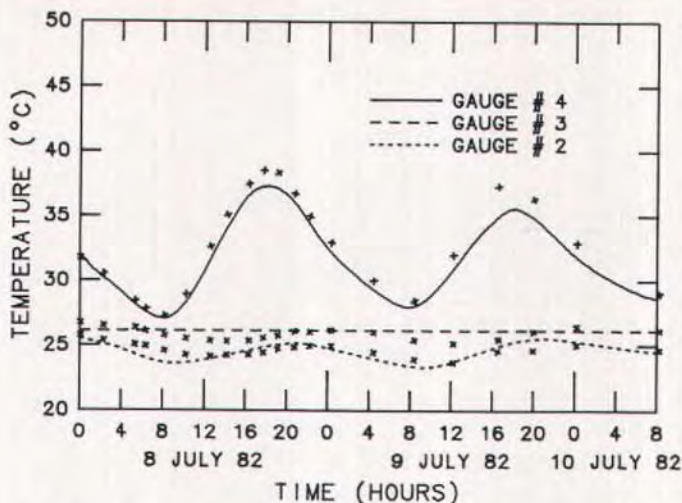


Fig. 2. Comparison of measured and computed temperature variations in web of Kishwaukee River Bridge.

flow simulation. Fig. 2 shows a comparison of measured and computed temperature changes at the top, middle and bottom of one of the webs, as explained previously. The plotted points represent measurements while the curves were extracted from computed results. Similar results were obtained for the other cross sections. The results were deemed of acceptable accuracy for the extension of model simulation to other bridges where hourly weather data were available.

WEATHER DATA COLLECTION INCLUDING SOLAR RADIATION

There are 89 weather stations in the United States where solar radiation intensities are recorded. Solar radiation has been recorded on an hourly basis at only 40 stations for varying periods starting in 1952.¹⁷ For all stations, however, meteorological measurements related to solar energy are available, which, in absence of radiation data, can be used to estimate instantaneous val-

ues of radiation. Data on hours of sunshine, or percentage of possible sunshine, are also widely available. Methods for the use of these data to estimate solar radiation can be found elsewhere.^{17,18}

Typical meteorological year tapes were prepared by the Sandia Laboratories in Albuquerque for the years 1954 to 1972.¹⁹ Data were prepared for 26 SOLMET stations and were processed as follows: Nine indices (total horizontal radiation; maximum and minimum, and mean of both dry bulb and dewpoint temperature, and the maximum and mean of wind speed) were identified as critical. For the preparation of the tapes, the data were weighted with the solar index as 50 percent and the rest of the factors as 50 percent. Typical months were identified by their closeness to long-term cumulative distribution functions.

The 26-station weather tape was used for this study to determine the magnitude and distribution of temperatures that can be expected in typical concrete bridge structures on days with extreme conditions at these locations. Each sta-



Fig. 3. Computed maximum temperature differences ($^{\circ}\text{C}$) of 2 m (6.56 ft) deep bridge structures (unsurfaced) located at different SOLMET stations.



Fig. 4. Computed maximum temperature differences ($^{\circ}\text{C}$) of 2 m (6.56 ft) deep bridge structures, with 50 mm (2 in.) blacktop, located at different SOLMET stations.



Fig. 5. Computed maximum temperature differences ($^{\circ}\text{C}$) of 2 m (6.56 ft) deep bridge structures, with 100 mm (4 in.) blacktop, located at different SOLMET stations.

tion is represented by 12 different months in its meteorological history for which a total of 8760 hours of climatic data are available. The list of names of stations appears in Table 1 as well as in Figs. 3 to 5.

SELECTION OF EXTREME DAYS

June 21 is the longest day of the year in the northern hemisphere and would, with absolutely clear sky conditions, exhibit the maximum total daily solar radiation of the year. Perfect clear sky conditions, however, are very rare in parts of the country, especially in some of the coastal regions. The conditions expected to produce maximum thermal loadings were therefore selected from the available data for the months of June and July, because those clearly contain the most favorable conditions for ex-

treme temperature differentials.

The three important meteorological parameters which govern the temperature distribution in concrete bridge structures are total solar radiation, air temperature variation during the day and the average wind speed. It is also important to know whether the three specific weather parameters can exhibit extreme values simultaneously to produce an absolute extreme temperature distribution. Emerson²⁰ determined that extreme environmental conditions were unlikely to occur on the same day in England.

The two most important weather factors to produce extreme temperature distributions are very high radiation accompanied by calm or very low wind speed. Solar radiation is the main source of heat energy to a bridge, and heat is lost back to the surroundings by reradiation and convection. The convective heat transfer coefficient is the smallest

Table 1. Number of days* when recorded weather data approaches the maximum temperature difference for each station.

Station and No.	Extreme day		Maximum temperature difference (°C)	No. of days
	Radiation (kJ/m ²)	Average wind speed (m/s)		
1 Fort Worth, TX	30943	4.8	24	5
2 Lake Charles, LA	28667	3.5	21	4
3 Columbia, MO	31021	3.0	25	5
4 Apalachicola, FL	29089	3.1	22	2
5 Miami, FL	25878	2.9	22	4
6 Brownsville, TX	28135	4.7	21	8
7 Charleston, SC	27661	2.8	24	2
8 Nashville, TN	29180	1.9	27	1
9 Dodge City, KS	34096	4.3	26	1
10 Caribou, ME	30794	1.8	23	2
11 Madison, WI	29367	1.6	24	1
12 El Paso, TX	33296	2.5	30	7
13 Albuquerque, NM	33818	1.8	30	1
14 Ely, NV	33226	3.7	30	4
15 Phoenix, AZ	32755	2.0	32	9
16 Santa Maria, CA	30924	3.2	26	3
17 Bismark, ND	30612	1.0	27	1
18 Great Falls, MT	31928	2.3	27	2
19 Medford, OR	31237	2.2	28	9
20 Seattle, WA	29225	1.7	27	1
21 Fresno, CA	33500	2.8	31	9
22 Cape Hatteras, NC	29343	3.2	23	2
23 Sterling, VA	28378	1.0	27	1
24 Boston, MA	33270	5.1	22	1
25 New York, NY	28753	3.3	20	1
26 Omaha, NB	30048	2.1	26	4

*These days are arbitrarily defined as having a total solar radiation no less than 97 percent of the extreme and an average wind speed of no more than 20 percent more than for the corresponding extreme day.

under calm conditions and increases rapidly with increased wind speed. The daily temperature variation has a smaller overall effect, presumably because of the very small volumetric specific heat of air relative to concrete. For instance, within the range of expected temperature variations of 14°F to 36°F (8°C to 20°C), the maximum temperature difference in a 6.56 ft (2 m) deep beam was increased by 3.6° (2°C).

On the other hand, an increase of wind speed from 0 to 11 mph (0 to 5 m/s), which is highly likely, would de-

crease the maximum temperature difference in the same beam by about 28.8°F (16°C). In order to determine the possible coexistence of the extreme environmental conditions on any given day, correlation analyses were done on the three important weather parameters.

Correlation Analysis

Table 2 shows the correlation coefficients for the different variables. As can be expected, there is a relatively good correlation between the total daily ra-

Table 2. Summary of correlation coefficients between the three governing weather parameters for June and July at 26 weather stations.

Total radiation vs temperature variation	Total radiation vs average wind speed	Temperature variation vs average wind speed
Mean 0.65	0.03	-0.20
Standard deviation 0.13	0.20	0.21

diation and temperature variation. This indicated that large temperature variations will accompany high daily radiation. Lower correlations were invariably found for coastal stations with a higher incidence of cloud cover. No correlation exists between average wind speed and either of the other two parameters.

Climatical Data for Thermal Analyses

Due to the complexity of the meteorological system, it is not justified to simply combine extreme climatical conditions in order to determine hypothetical maximum temperature differences through a concrete structure. Provision for such a hypothetical condition can lead to overdesign and unnecessarily increase construction costs. An attempt was therefore made to determine realistic extreme conditions.

Data for two actual days recorded at each weather station during June and July were used to calculate the corresponding temperature distributions. The first day represents the day with the highest total solar radiation during the typical meteorological year. The second day was selected from those during the typical year for which at least 95 percent of the radiation of the first day was recorded. The main priority for the choice of the second day was a combination of very low average wind speed and high total radiation. In making the selection, very little attention was given to temperature variation during the day.

Evaluation of Maximum Radiation Values

The method by Threlkeld¹⁸ and Duffie and Beckman¹⁷ is generally used in solar engineering for the theoretical determination of instantaneous beam as well as diffuse solar radiation. In order to evaluate the measured maximum radiation values, the solar radiation measurements at the different SOLMET stations were compared with the theoretical clear sky distribution on June 21. On average, theoretical total values are 2.5 percent less than those obtained from the hourly data. A larger deviation was obtained at coastal areas where absolutely clear sky conditions are rare.

When comparing the statistical average daily radiation at the different stations with the corresponding maximum reported values, it is evident that the measured values are well above average. The recorded radiation values are therefore considered suitable to represent the upper limit of radiation at the respective stations.

DATA FOR THERMAL ANALYSES

Thermal loading parameters that are specifically relevant to the summer extremes at the different SOLMET stations were deduced from the available meteorological data. Also, the attenuation of the temperatures through the structural concrete from the upper surface and specifically the influence of the

Table 3. Thermal properties of concrete used in thermal analyses.

Property	Concrete	Bitumen	Air
Density (kg/m ³)	2480	2300	1.3
Specific heat (J/kg °C)	922	840	1006
Conductivity (W/m °C)	1.384	0.744	0.023
Absorptivity	0.7	0.9	

Surface Heat Transfer

Heat transfer on the top surface:

$$h_t = 13.5 + 3.88v \text{ (W/m}^2 \text{ °C)}$$

where v = wind speed (m/s)

For the bottom exposed surface a value of 0.45 of the top surface heat transfer was used. This is based on results of tests by Emerson.²⁵

For inside surfaces of flanges and partially protected lower surfaces, a value of 0.2 of top surface heat transfer was used.

thickness of existing bituminous surfacing were determined. Finally, deformation and stress criteria, which can be used as guidance for the incorporation of thermal loading into the bridge design process, were developed from the resulting analyses.

In the theoretical process of thermal analysis, where only limited data are available, the values of parameters have to be reliable. Assumptions made in the theoretical analysis are discussed in the following categories: climatical data, thermal properties of structural material and starting conditions in the structure.

Climatical Data

The ambient conditions as measured at the 26 SOLMET stations were used for the determination of the variation in thermal loading throughout the United States. The time was recorded at all the stations according to the solar time system, which is a more standardized approach than the regular time zone system. Wind speed was measured about 33 ft (10 m) above ground. To allow for the probable reduced exposure of bridges at heights which would normally be between 6 and 26 ft (2 and 6 m)

above ground and possible partial protection by the surroundings, the wind speed values used in the thermal analyses were reduced to 80 percent of those recorded. All the other weather data were used exactly as recorded.

Thermal Properties of Structural Material

A range of thermal properties is reported in the literature. Priestley²¹ performed a parametric study on the influence of different thermal properties of concrete on the response of bridge structures. The influence of changes in these properties within the range of experimentally determined values was found to be small. One exception, however, is the absorptivity of the exposed upper surface. This factor will be discussed in more detail later in this paper. The values for different thermal properties and variables that were used in the thermal analyses are presented in Table 3.

Starting Temperature Distribution

A slightly higher temperature of 3 to 5°F (2 to 3°C) normally exists at the

upper parts of the deck compared to the lower parts at the minimum temperature distribution during the night. For these analyses, however, a uniform starting temperature distribution was assumed. The discrepancy between measured and assumed starting temperatures can be diminished by repeating the thermal analysis for the same day, using the distribution determined for the end of the initial period as the starting distribution of the second analysis.

THERMAL ANALYSES FOR 26 SOLMET STATIONS

The linear heat flow model described earlier was used for a variety of thermal analyses. In four series of analyses, concrete structures of different depths were analyzed with plain concrete upper surfaces, and with 2 in. or 4 in. (50 mm or 100 mm) thick bitumen blacktops, respectively, under the specific weather conditions at each of the 26 SOLMET stations. In the first series, the weather data of two different days (described earlier) were used to compute the temperature distribution through a 6.56 ft (2 m) deep structure.

The day which gave rise to the larger temperature difference through the structures at each of the stations was used for the analysis of structural concrete of 3.28 ft (1.0 m) thickness in the second series, 1.64 ft (0.5 m) thickness in the third series, and a structure with an air cavity in the fourth series. The thickness of the deck slab was 7.87 in. (0.200 m), the bottom slab 5.91 in. (0.150 m) and the overall thickness was 3.28 ft (1.0 m) in the last case.

RESULTS OF THERMAL ANALYSES OF SOLID STRUCTURES

The comparatively low conductivity of concrete does not allow significant

heat penetration from the top to depths of 3 ft (1 m) or more. Minor temperature increases are also experienced in the bottom 8 in. (0.2 m) of the structure.

The geographical variation of the maximum temperature differences through the 6.56 ft (2 m) structure with an exposed concrete top surface, 2 and 4 in. (50 and 100 mm) blacktop, respectively, are presented in Figs. 3 to 5. The three sets of analyses show similar variations of values with location and show a decrease in temperature differences with an increase in blacktop thickness.

Analysis of the geographical presentation of the results can lead to the identification of regions with similar thermal loadings. The stations representing the desert and semidesert parts of the country, e.g., western Texas, New Mexico, Arizona, Nevada and eastern California, exhibited the highest temperature differences between the top and bottom parts of the bridge structures. The values obtained for structures with no blacktop in this region (Fig. 3) are between 54 and 58°F (30 and 32°C). On the other hand, coastal weather parameters moderate the differences along the coast line. The frequent occurrence of high wind speeds at Dodge City, Kansas, where the highest one day radiation of all the SOLMET stations was recorded, moderated the calculated temperature difference of an unsurfaced bridge structure at 47°F (26°C).

The climatical data for the stations in the Midwest produced very similar results with temperature differences ranging from 43 to 47°F (24 to 26°C). Nashville, Tennessee, with a maximum temperature difference of 49°F (27°C), can also be included in this region. Thermal analyses for all the stations along the Gulf Coast, including Miami, yielded temperature differences of 38 to 40°F (21 or 22°C). The recorded solar radiation at these stations were medium to low. The fact that this part of the country has the lowest atmospheric clearness

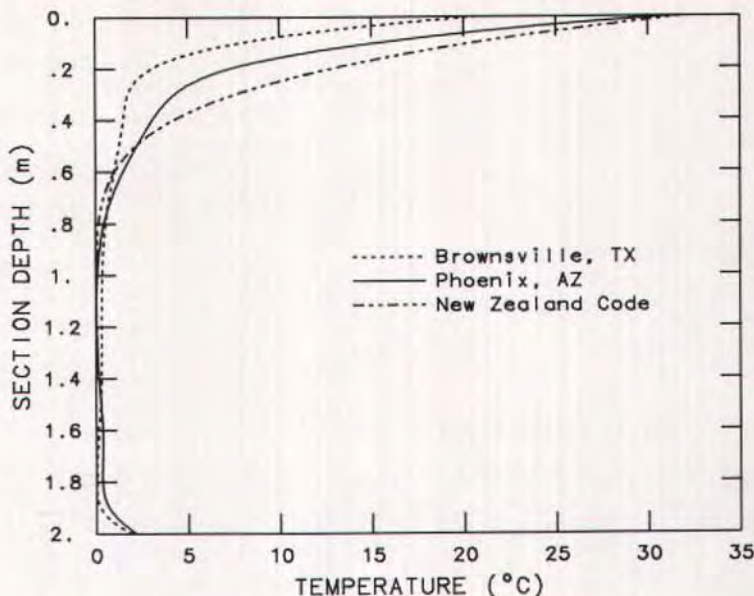


Fig. 6. Maximum temperature distributions in 2 m (6.56 ft) deep bridge structures (unsurfaced).

number supports the results. The constant Gulf Coast winds of between 4.5 and 13 mph (2 and 6 m/s) resulted in the reduction of maximum temperature differences.

Table 1 indicates the number of days in the typical year that would approach the maximum calculated temperature differences for each station. These days were arbitrarily defined as having a total solar radiation of at least 97 percent of the day which caused the maximum condition together with an average wind speed of no more than 20 percent higher than the average wind speed of the reference day. For the vast majority of the stations, the extreme conditions were very seldom approached during June and July.

Weather data for the stations at Brownsville, Texas; El Paso, Texas; Phoenix, Arizona; Medford, Oregon; and Fresno, California, show a probable incidence of 7 to 9 days during the 2 month period with conditions favorable

for large temperature differences. Brownsville is the only station of this group for which the computed maximum temperature difference was lower than 50°F (28°C) for the concrete structure with no blacktop. At the other stations, extreme conditions were approached between 1 and 5 days per year. Distress, in the form of unwanted cracking, is more likely to occur with repeated high thermal loadings at the first-mentioned stations.

SENSITIVITY ANALYSES

As stated earlier, the important weather parameters influencing temperature differences are radiation and wind speed, while the ambient temperature variation has a smaller influence. Two sets of sensitivity analyses were performed on a 6.56 ft (2 m) deep bridge using the weather data of Stations 4 and 13. The results indicate that a 10 percent increase in the total radiation would in-

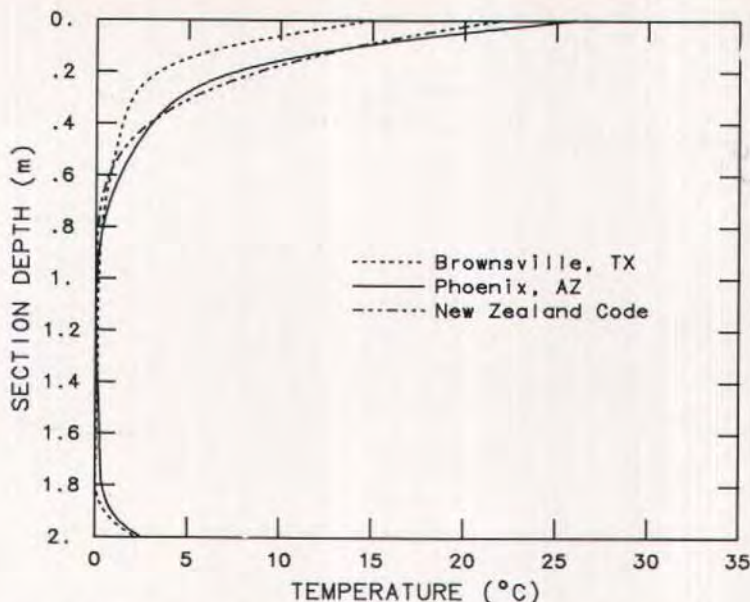


Fig. 7. Maximum temperature distributions in 2 m (6.56 ft) deep bridge structures, with 50 mm (2 in.) blacktop.

crease the maximum temperature difference by about 5.4°F (3°C).

The total radiation received by the structure is directly related to the absorptivity of the top surface. A variation in this parameter of up to 20 percent can exist for the same structure depending on the top surface. If the wind speed increases by 2.2 mph (1 m/s), the temperature difference is reduced by about 2.7°F (1.5°C). Average wind speed differences of up to 6.7 mph (3 m/s) are quite common on days with very high total radiation. When different days with extreme conditions are compared, the total ambient temperature changes compare within 2 to 7°F (1 to 4°C) and the related temperature differences in bridge structures correspond within 2°F.

VERTICAL TEMPERATURE DISTRIBUTIONS

The wide variety of thermal conditions which exist throughout the United

States was reflected in the maximum temperature difference results obtained for webs. The variation in temperature distributions under these conditions and especially the bridge response to these temperature loadings are important in bridge analysis. In order to determine the vertical temperature distribution in a typical web structure, the 6.56 ft (2 m) deep rectangular section described previously was analyzed.

The SOLMET weather stations at Brownsville, Texas, and Phoenix, Arizona, represent the lower and upper limits of the computed maximum temperature differences (Figs. 3 to 5). The temperature distributions associated with the weather data of the other stations fall mainly within the bounds set by these two stations. The temperature distributions obtained from the weather data of these two stations are illustrated in Figs. 6 to 8. The graphs represent the thermal analyses for the structures with an exposed concrete upper surface, 2 in. (50

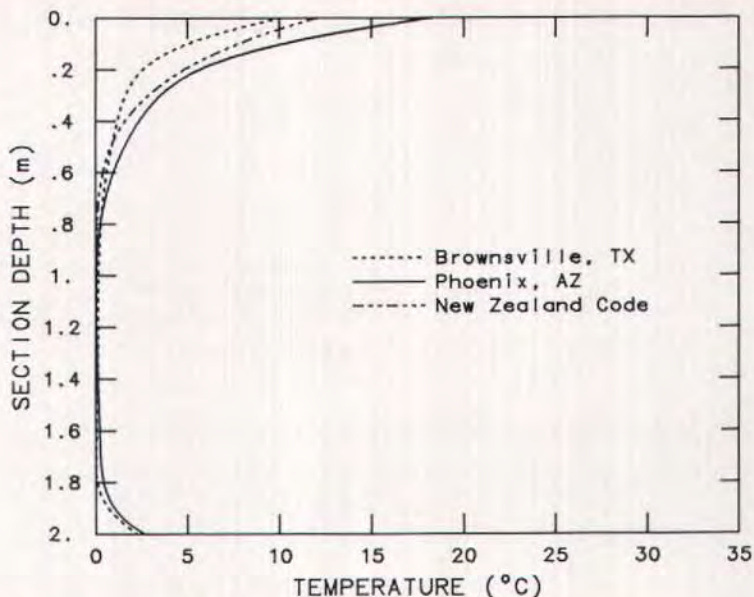


Fig. 8. Maximum temperature distributions in 2 m (6.56 ft) deep bridge structures, with 100 mm (4 in.) blacktop.

mm) bitumen blacktop and 4 in. (100 mm) blacktop, respectively, in comparison with the design temperature distribution as specified by the New Zealand Ministry of Works.³ This temperature distribution was developed after model tests as well as extensive analyses of various prototype bridges in New Zealand. (The small temperature distribution function of the New Zealand code for the bottom of the section is omitted for clarity.)

Although the temperature distributions for the two weather stations do not differ significantly, the horizontal separation in the top 8 in. (0.2 m) of the structure is between 7 and 18°F (4 and 10°C) for the unpaved structures. Differences of this magnitude in temperature distribution can cause substantial differences in bridge response.

The computed temperature distributions have a notably larger gradient than the curve of the New Zealand Code. The maximum temperature distribution is a function of the blacktop thickness.

The blacktop serves as insulation and, due to thermal lag, the maximum temperature distribution occurs at a later stage in the concrete structure when it is covered with a thicker pavement. Maximum temperature distributions were generally recorded at 1400, 1530, and 1700 hours local solar time for the unsurfaced structure, 2 and 4 in. (50 and 100 mm) blacktop structures, respectively.

The computed temperature distribution for Phoenix, Arizona, closely resembles the corresponding curve of the New Zealand Code for the structure with 2 in. (50 mm) of blacktop. For the unsurfaced structure, the computed curve is slightly below that of the New Zealand Code, while for the structure with the 4 in. (100 mm) bitumen pavement, the computed temperatures are slightly above the Code values.

The bottom portion of the New Zealand curve is not shown in these figures because of the clutter it would create. It appears in Fig. A1, showing a lower

surface temperature 2.7°F (1.5°C) higher than the web temperature 8 in. (0.2 m) above the soffit. The computed soffit temperature differences, however, ranged between 3.6 and 5.4°F (2 and 3°C) above the web temperatures. The constant temperature region in the web was reached at about the same 8 in. (0.2 m) height above the soffit. The temperature differentials for a bridge with structural depth of 20 in. (0.5 m) do not reach the maximum values obtained for the deeper structures and the computed soffit temperatures for this structure are also slightly lower.

INDUCED CURVATURES OF BRIDGE SECTIONS

Temperature loadings do not induce the same response in all types of bridges. The response is mainly dependent on the type of cross section of a superstructure, the span configuration, the degree of fixity and the bridge material.

In this section, an attempt will be made to generalize the response in typical box girder cross sections depending on their depths and to obtain a general thermal curvature for the typical sections depending on the specific thermal loading. A variety of bridge cross sections have been analyzed elsewhere,⁶ but only the general box girder cross section is discussed here.

Constant depth box girder bridges are used for longer span bridges with span lengths normally in the range of 78 to 250 ft (24 to 75 m). A wide range of cross sections are used in practice and, although some basic dimensional limits are set by the AASHTO Code,¹ the different structural requirements as well as aesthetic considerations make it difficult to generalize cross sections. However, similar thermal curvature responses were found for different structures with the same section depth. The response of 18 existing box girder bridges were

computed using the thermal analysis program.⁶ The bridges studied included the Kishwaukee River Bridge,^{15,16} the experimental segmental bridge at Penn State,²² and others from various published and unpublished sources.

The temperature distributions from Brownsville, Texas (Station 6), and Phoenix, Arizona (Station 15), were used for the analyses, since these stations produced the lowest and highest temperature gradients, respectively, of the 26 stations considered. Provision was made for the fact that at extreme conditions, temperatures in the slab above the air cavity are a few degrees higher than those at the same height in the web sections and that the temperature gradient in the slab is also smaller.^{3,11}

For each of the box girder bridges, only the most typical section was analyzed. The thermal curvatures for the 18 bridges computed from the temperature distributions at Stations 6 and 15 are shown in Figs. 9 and 10. Only the plotted points for the unsurfaced bridge are shown.

The relatively small scatter of points made it possible to represent the values with a third order polynomial. The presentation of the data points by polynomials can be slightly improved by dividing the depth range into two sets, 3 to 8 ft, and 8 ft and above (1 to 2.5 m and 2.5 m and above), for two individual sets of equations.

In order to compute the top and bottom flange stresses of bridge decks, values of residual stresses must also be known. The residual stress is the thermally induced stress at the soffit of a statically determinate member [see Fig. A2(d)]. A linear function depending on the deck depth was found to yield acceptable results. The residual stresses should not be taken to be particularly accurate because they were derived from a one-dimensional heat flow analysis applied to a two-dimensional cross section, but the stresses should properly indicate trends.

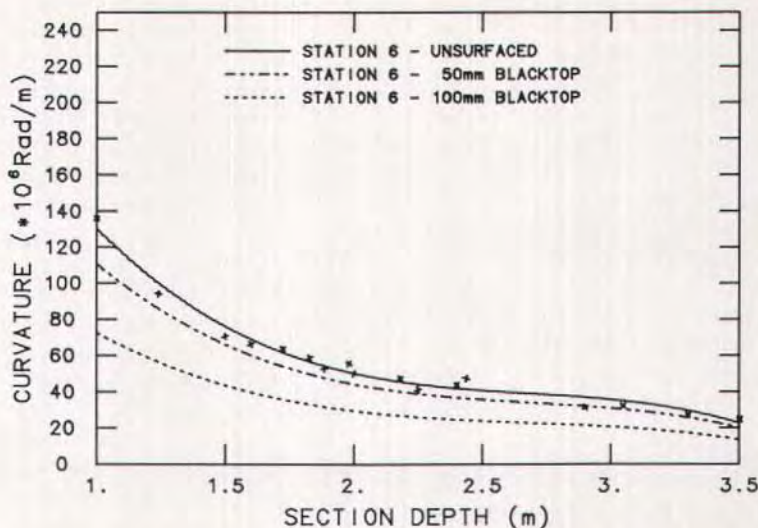


Fig. 9. Temperature induced curvatures for box girders subjected to Station 6 weather conditions.

The different curvature and residual stress polynomials are as follows:

Station 6 (SI units)

Unsurfaced

$$\phi_T = 374 - 358d + 130d^2 - 16.2d^3$$

$$f_r = -1.3 + 0.074d$$

50 mm blacktop:

$$\phi_T = 307 - 287d + 103d^2 - 12.8d^3$$

$$f_r = -1.2 + 0.045d$$

100 mm blacktop:

$$\phi_T = 198 - 184d + 66.4d^2 - 8.2d^3$$

$$f_r = -0.92 + 0.015d$$

Station 15

Unsurfaced:

$$\phi_T = 638 - 585d + 208d^2 - 25.4d^3$$

$$f_r = -2.1 + 0.18d$$

50 mm blacktop:

$$\phi_T = 522 - 455d + 157d^2 - 18.8d^3$$

$$f_r = -2.0 + 0.12d$$

100 mm blacktop:

$$\phi_T = 347 - 294d + 100d^2 - 11.9d^3$$

$$f_r = -1.6 + 0.09d$$

Note: 1 rad/m = 0.3048 rad/ft; 1 ksi = 6.895 MPa = 6.895 N/mm²; 1 m = 3.281 ft = 39.37 in.

where

ϕ_T = curvature due to temperature differences (rad/m x 10⁶)

f_r = residual stress (MPa) at bottom of section, determinate member

d = girder depth (m)

Station 6 (Imperial units, converted from SI units)

Unsurfaced:

$$\phi_T = 114 - 33.3D + 3.68D^2 - 0.140D^3$$

$$f_r = -189 + 3.27D$$

2 in. blacktop:

$$\phi_T = 93.6 - 26.7D + 2.92D^2 - 0.110D^3$$

$$f_r = -174 + 1.99D$$

4 in. blacktop:

$$\phi_T = 60.4 - 17.1D + 1.88D^2 - 0.071D^3$$

$$f_r = -133 + 0.66D$$

Station 15

Unsurfaced

$$\phi_T = 194 - 54.3D + 5.89D^2 - 0.219D^3$$

$$f_r = -304 + 7.96D$$

2 in. blacktop:

$$\phi_T = 159 - 42.3D + 4.45D^2 - 0.162D^3$$

$$f_r = -290 + 5.30D$$

4 in. blacktop:

$$\phi_T = 106 - 27.3D + 2.83D^2 - 0.103D^3$$

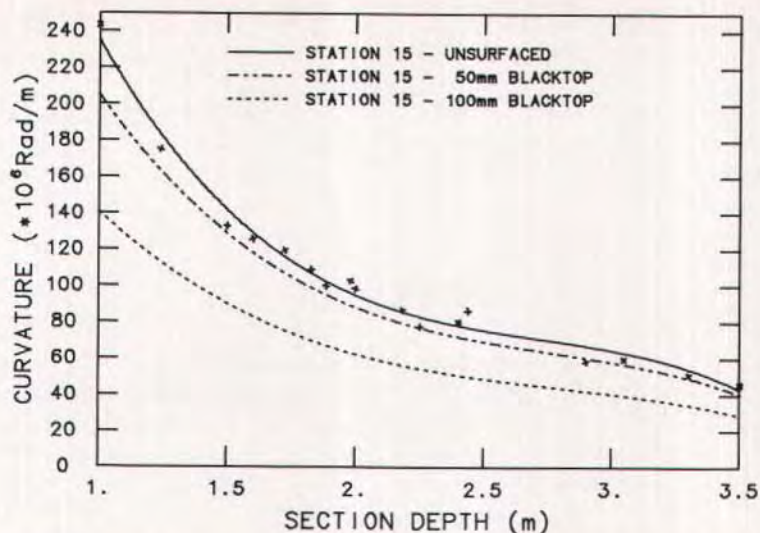


Fig. 10. Temperature induced curvatures for box girders subjected to Station 15 weather conditions.

$$f_r = -2.2 + 3.98D$$

where

ϕ_T = curvature due to temperature differences (rad/ft x 10⁶)

f_r = residual stress (psi) at bottom of section, determinate member

D = girder depth (ft)

APPLICATION TO PRETENSIONED BRIDGES

The temperature differentials which are computed and observed in concrete bridges lead to significant stresses and deformations. The temperature related stresses are often of the same general magnitude as the allowable service load stresses, as the stresses shown in Appendix A demonstrate.

However, it is suggested that the bridge design profession move very slowly in incorporating thermal stress calculations and stresses into the design process. While it is clear that thermal stresses and deformations have damaged a few structures,²³ it appears that these are a relatively few cases in a very large bridge

population.

One result of the restraint of thermal deformations is the development of positive moments at interior supports (see Appendices A and B). The composite pretensioned I-girder bridge which is made continuous by means of deck reinforcement and compression concrete cast between the girder ends would appear to be especially vulnerable to damage. There is no dead load negative moment at the interior supports, and there may be no positive moment connection of any kind. Moments may be induced as a result of creep and shrinkage strains, but these moments can be either positive or negative, depending on many variables.²⁴

Thus, the thermal deformations would be expected to cause significant positive moments and, consequently, cracking at interior supports, but this damage does not appear to have occurred in this type of bridge. If the thermal deformations cause significant positive moment cracking at the interior supports, the forces are temporarily relieved. However, if the cracks are of any size, they will not close very well when the thermal deformations are removed, and an accumulation of

local crushing damage would be expected. This does not appear to have been reported.

The recommendation that changes be introduced very cautiously is based on the observation that very little damage

has occurred in bridges which can be traced directly to thermal stresses and deformations.

It is clear that thermally induced cracking has damaged some post-tensioned box girder bridges.²³

CONCLUSION

Theoretical methods are available to generate values for weather parameters that can be used for the successful thermal analysis of bridge structures at any location in the United States for which only limited weather data exist. A wide range of thermal loadings will be produced due to the large variation of climatical parameters. It is evident that the combination of weather conditions which will result in an extreme temperature distribution in bridge structures would be clear days with high solar radiation and very low wind speeds.

A large range in air temperature also increases the differential temperature in the bridge, but this is a smaller factor. The data for the 26 SOLMET stations

were successfully used to compute probable temperature distributions in bridges located at different parts of the United States. The geographical region at highest risk for stress due to thermal loadings was identified as the desert Southwest. In turn, the effects of nonlinear temperature distributions in bridges along the coast are much less important in design.

The analysis of bridge structures for thermal loadings is appreciably simplified by the use of the curvature-depth and the residual stress-depth relationships. If the magnitude of thermal stresses or the size of the project warrants more in-depth heat flow analyses, the equations would give acceptable accuracy for preliminary design purposes.

REFERENCES

1. American Association of State Highway and Transportation Officials (AASHTO), *Standard Specifications for Highway Bridges*, 13th Edition, 1983.
2. British Standard BS 5400, *Steel, Concrete and Composite Bridges, Part 2*, British Standards Institute, 1978.
3. New Zealand Ministry of Works and Development, *Highway Bridge Design Brief, Issue C*, Office of the Chief Civil Design Engineer, Wellington, New Zealand, 1973, 51 pp., Amended in August 1976.
4. Imbsen, R. A., Vandershaf, D. E., Schamber, R. A., and Nutt, R. V., "Thermal Effects in Concrete Bridge Superstructures," National Cooperative Highway Research Program Report 276, Transportation Research Board, Washington, D.C., September 1985, 99 pp.
5. AASHTO, "Guide Specifications—Thermal Effects in Concrete Bridge Superstructures," in preparation.
6. Potgieter, I. C., and Gamble, W. L., "Response of Highway Bridges to Non-linear Temperature Distributions," Civil Engineering Studies, Structural Research Series 505, University of Illinois, 1983, 219 pp.
7. Priestley, M. J. N., "Design of Concrete Bridges for Temperature Gradients," *ACI Journal*, V. 75, No. 5, May 1978, pp. 209-217.
8. Cooke, N., Priestley, M. J. N., and Thurston, S. J., "Analysis and Design of Partially Prestressed Concrete Bridges Under Thermal Loading," *PCI JOURNAL*, V. 29, No. 3, May-June 1984, pp. 94-114.

9. Lanigan, A. G., "The Temperature Response of Concrete Box Girder Bridges," PhD Thesis and Report No. 94, School of Engineering, University of Auckland, Auckland, New Zealand, September 1973.
10. Bryant, A. H., Buckle, I. G., and Lanigan, A. G., "Prediction of Temperatures in Box Girder Bridges," Proceedings, 7th Australian Road Research Board Conference, V. 7, Part 7, 1974, pp. 296-308.
11. Hunt, B., and Cooke, N., "Thermal Calculations for Bridge Design," Proceedings, ASCE, *Journal Structural Division*, V. 101, No. ST9, September 1975, pp. 1763-1781. (See also Discussion, V. 102, No. ST6, June 1976, pp. 1277-1279, V. 103, No. ST4, April 1977, p. 919.)
12. Thurston, S. J., "Thermal Stresses in Concrete Structures," PhD Thesis and Research Report 78-21, Department of Civil Engineering, University of Canterbury, Christchurch, New Zealand, November 1978.
13. Hirst, M. J. S., "Thermal Loading of Concrete Bridges," Proceedings, International Conference on Short and Medium Span Bridges, Toronto, 1982, V. 1, pp. 115-124.
14. Elbadry, M. M., and Ghali, A., "Temperature Variations in Concrete Bridges," *Journal of Structural Engineering*, V. 20, No. 10, October 1983, p. 2355-2374.
15. Russell, H. G., Shiu, K. -N., Gamble, W. L., and Marshall, V., "Measured and Calculated Time-Dependent Deformations in a Post-Tensioned Concrete Box Girder Bridge," Proceedings, International Conference on Short and Medium Span Bridges," Toronto, 1982, V. 1, pp. 439-450.
16. Marshall, V., and Gamble, W. L., "Time Dependent Deformations in Segmental Prestressed Concrete Bridges," Civil Engineering Studies, Structural Research Series No. 495, UIIU-ENG-81-2014, University of Illinois at Champaign-Urbana, Urbana, IL, October 1981, 242 p.
17. Duffie, J. A., and Beckman, W. A., *Solar Energy Thermal Processes*, John Wiley & Sons, New York, NY, 1980.
18. Threlkeld, J. L., *Thermal Environmental Engineering*, Prentice Hall, Inc., Englewood Cliffs, NJ, 1970.
19. Typical Meteorological Year Tapes (TMY) SOLMET, Sandia Laboratories, Albuquerque, NM.
20. Emerson, M., "Extreme Values of Bridge Temperatures for Design Purposes," TRRL Report LR744, Department of Environment, England, 1976.
21. Priestley, M. J. N., "Design Thermal Gradients for Concrete Bridges," *New Zealand Engineering*, V. 31, No. 9, September 1976, pp. 213-219.
22. Hoffman, D. C., McClure, R. M., and West, H. H., "Temperature Study of an Experimental Segmental Bridge," *PCI JOURNAL*, V. 28, No. 2, March-April 1983, pp. 78-97.
23. Podolny, Walter, Jr., "The Cause of Cracking in Post-Tensioned Concrete Box Girder Bridges and Retrofit Procedures," *PCI JOURNAL*, V. 30, No. 2, March-April 1985, pp. 82-139.
24. Mossiosian, V., and Gamble, W. L., "Time Dependent Behavior of Noncomposite and Composite Prestressed Concrete Structures Under Field and Laboratory Conditions," Civil Engineering Studies, Structural Research Series No. 385, University of Illinois at Urbana-Champaign, Urbana, IL, May 1972, 517 pp.
25. Emerson, M., "The Calculation of the Distribution of Temperature in Bridges," TRRL Report LR561, Department of Environment, England, 1973.

* * *

NOTE: Discussion of this article is invited. Please submit your comments to PCI Headquarters by April 1, 1990.

APPENDIX A — EXAMPLE OF TEMPERATURE INDUCED STRESS CALCULATIONS (EXAMPLE IN SI UNITS)

A simple example is used to show the analysis steps and the general results of applying a nonlinear temperature distribution to an elastic, uncracked concrete member. A rectangular section is used. More typical sections such as T-sections can be handled, but the amount of arithmetic increases significantly and the general pattern of response remains the same.

Fig. A1 shows the section, and the temperature distribution prescribed by the New Zealand Ministry of Works and Development.³ The fifth order curve has been shown to be a reasonable approximation of measured distributions, and the 32°C differential is appropriate for New Zealand. This temperature distribution produces stresses and deformations in the member which can be superimposed with those from other causes, within the limits of elasticity. These temperature stresses can be computed by a series of steps, with the components added to produce total stresses.

Step 1 — Compute stresses assuming deformations caused by temperature increase are completely restrained. The stress at any point is then:

$$f_t = T(y) \alpha_c E_c$$

where

$T(y)$ = temperature change at section considered

α_c = coefficient of thermal expansion of material

Note: The metric (SI) values of E_c and C_t were purposely chosen to be round whole numbers in order to simplify the arithmetic so that the main attention could be focused on the process. The values are reasonable for concrete.

Conversion factors: 1 in. = 25.4 mm; $E_c = 25$ kN/mm² = 3.63×10^6 psi; 1 ksi = 6.895 MPa; $C_t = 10 \times 10^{-6}/^\circ\text{C} = 5.56 \times 10^{-6}/^\circ\text{F}$; $\phi_T = 103.2 \times 10^{-6}$ rad/m = 2.621×10^{-6} rad/in.; $1^\circ\text{C} = 1.8^\circ\text{F}$ differential.

E_c = Young's modulus of material

Fig. A2(b) shows the stresses resulting in a 1700 mm deep section from the temperature distribution shown in Fig. A1, assuming the case of complete restraint of thermal strains. The top fiber stress is -8.0 N/mm². The stresses have been resolved into the two force components also shown in Fig. A2(b).

Step 2 — The stresses are, of course, not fully restrained, and this is taken into account by applying the two compression forces as tension forces acting at the same locations. Stresses from these two forces are computed using the familiar equation:

$$f = P/A \pm My/I$$

and the resulting stress distribution is shown in Fig. A2(c). This distribution is linear.

Step 3 — The stresses shown in Figs. A2(b) and (c) are then added, giving the distribution shown in Fig. A2(d). This final stress distribution is in internal equilibrium, with the stresses producing neither net moment nor net thrust.

If the member is statically determinate, there are no other forces to be considered, although there are also curvatures. If the original temperature distribution had been linear, the stress components would have completely canceled out, although there still would have been curvatures.

Step 4 — The curvature induced can be found by converting the stresses shown in Fig. A2(c) to strain and dividing the algebraic difference between top and bottom fiber strains by the section depth, or by dividing the net moment caused by the forces shown in Fig. A2(b) by EI . For this particular example, the curvature is:

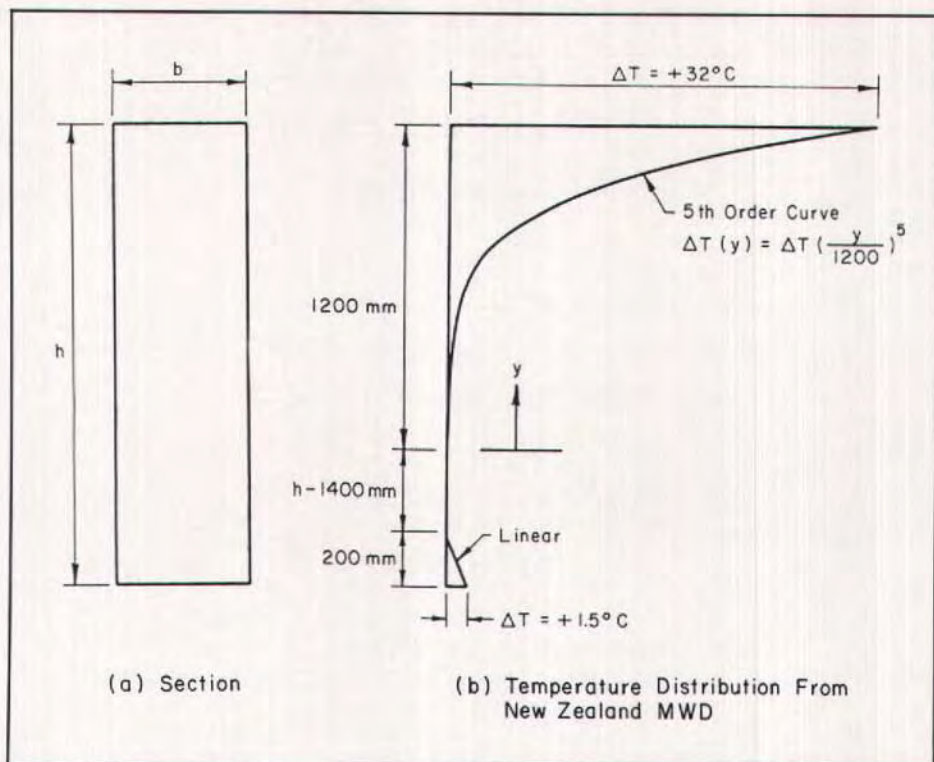


Fig. A1. Rectangular section and nonlinear temperature distribution.

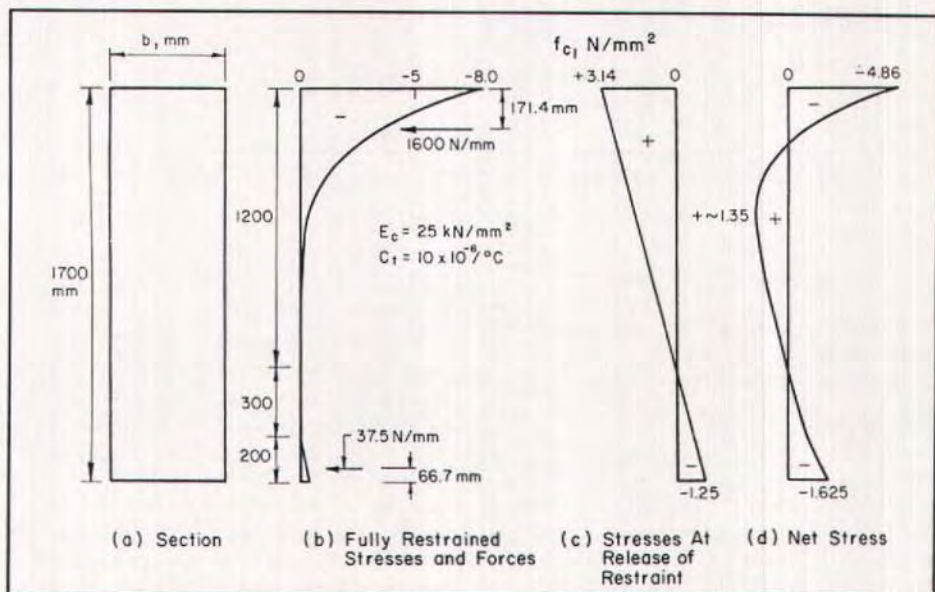
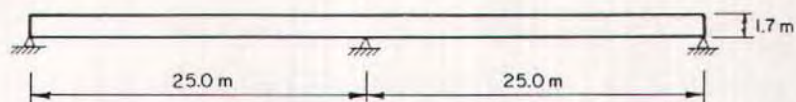
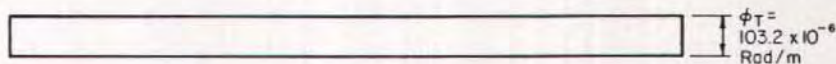


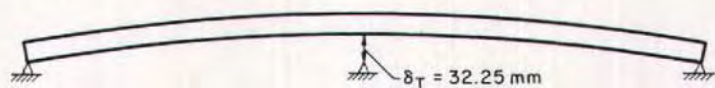
Fig. A2. Temperature stresses in determinate member.



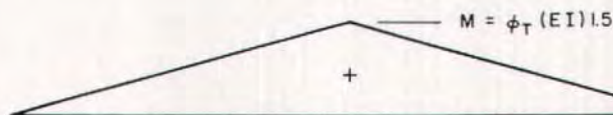
(a) Example Two-Span Structure



(b) Curvature Due To Temperature Gradient



(c) Unrestrained Deformation of Beam



(d) Moments Due To Restraining Forces At Central Support

Fig. A3. Temperature induced moments in two-span continuous beam.

$$\phi_T = 103.2 \times 10^{-6} \text{ rad/m}$$

Step 5 — The top side of the member is the heated side, so the member bows or hogs up. The upward deflection for this prismatic member is:

$$\delta_T = \phi_T (\text{Span})^2 / 8$$

If the member is statically indeterminate, this tendency to camber upward produces additional stresses and forces in the member. Fig. A3 shows an assumed two-span continuous member,

with spans of 25 m, along with the curvature due to the temperature gradient. If the structure is made determinate by removing the central support, it will be found that the member cambers up 32.25 mm away from the central support, or at least would if it were weightless.

Step 6 — A force is required to push the beam back down to the central support, and this causes the moment diagram shown in Fig. A3(d). The moment is independent of the length of the

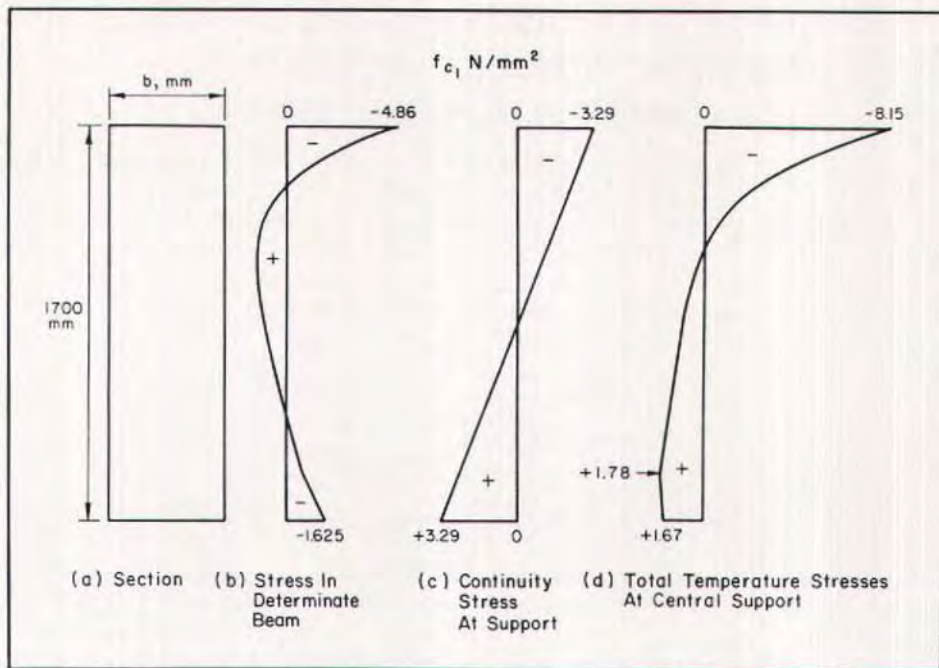


Fig. A4. Temperature stresses at interior support, two-span beam.

member. This moment diagram is superposed with those from the other dead and live loads in a determination of total stress. The 1.5 factor in the equation for the moment due to the restraining force, $\phi_T(EI)1.5$, is specific to a two-span beam and will be smaller for structures with more spans.

Step 7 — Fig. A4 completes the superposition process to find the total temperature induced stress at the central support. Fig. A4(b) shows the stress distribution in the determinate beam, and Fig. A4(c) shows the stress distribution at the central support caused by the continuity moment. Fig. A4(d) shows

the total stresses over the depth of the section at the central support.

It will be noted that these stresses generally are in opposition to those caused by the gravity load forces, but that they are generally additive to stresses caused by post-tensioning. At a midspan section, the continuity stresses would be half those shown here, but they are additive to the gravity load stresses. It is thus not always clear which section might be hurt worse by temperature induced stresses, but it is clear that these elastic stresses may be a major fraction of the usual service load allowable stresses.

* * *

APPENDIX B — EXAMPLE CALCULATION OF THERMAL FORCES IN BOX GIRDER (EXAMPLE IN IMPERIAL UNITS)

Consider the cross section of the Kishwaukee River Bridge, shown in Fig. 1. Ignore the fact that the bottom slab of the box is thicker near the piers so that a prismatic section can be considered. With the minimum bottom slab thickness, the member has the following properties:

$$I = 32,005,000 \text{ in.}^4$$

$$A = 11,595 \text{ in.}^2$$

$$c_t = 51.216 \text{ in.}; c_b = 88.534 \text{ in.}$$

$$\text{Total depth} = 139.75 \text{ in.} = 11.646 \text{ ft} = D$$

The concrete had $E_c = 4500$ ksi at 6 months, for specimens stored outdoors with the bridge.

Consider a three-span bridge, with end spans of 170 ft and an interior span of 250 ft, as shown in Fig. B1(a). There is a 2 in. asphalt topping.

If the bridge is in the desert South-

west, the Station 15 (Phoenix) data can be used to compute the thermal curvature and residual stress. The curvature can also be obtained from Fig. 10.

$$\begin{aligned} \phi_T &= 10^{-6} [159 - 42.3D + 4.45D^2 - 0.162D^3] \text{ rad/ft} \\ &= 10^{-6} [159 - 42.3 \cdot 11.646 + 4.45 \cdot 11.646^2 - 0.162 \cdot 11.646^3] \\ &= 14.039 \cdot 10^{-6} \text{ rad/ft} = 1.170 \cdot 10^{-6} \text{ rad/in.} \end{aligned}$$

$$f_r = -290 + 5.30D = -290 + 5.30 \cdot 11.646 = -228 \text{ psi}$$

The curvature corresponds to a negative moment, producing upward deflection, or hogging. If the same approach were used as was shown in Appendix A, it would be found that the 590 ft long member would camber upward 0.6109 ft at the middle of the interior span, and by some lesser amount at the interior supports. Also, the force required to restrain the movement at the interior supports to zero could be found.

A different approach will be used in this example. The application of a pos-

Metric (SI) conversion factors: 1 in. = 25.4 mm; 1 ft = 0.3048 m; 1 ksi = 6.895 N/mm² = 6.895 MPa; 1 x 10⁻⁶ rad/in. = 39.37 x 10⁻⁶ rad/m; 1 kip-in. = 0.11298 kN-m.

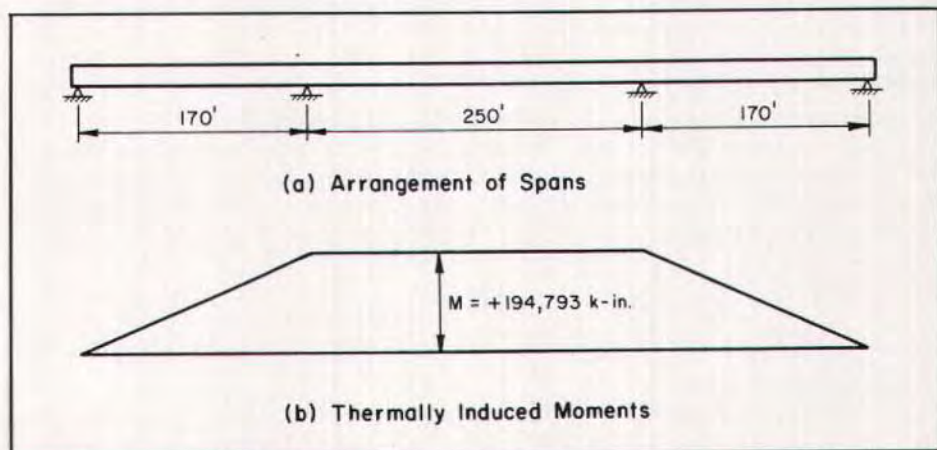


Fig. B1. Example of moments in three-span bridge.

itive moment equal to $\phi_r * EI_c$ to both ends of a member will exactly counteract the thermal curvature, resulting in a straight member. This is in effect a fixed end moment, and the most efficient way of dealing with this is to make the member determinate by breaking it into three separate spans.

Each span then has fixed end moments equal to:

$$\begin{aligned}\phi_r * EI_c &= 1.170 * 10^{-6} \text{ rad/in.} * 4500 \\ &\quad \text{ksi} * 32,005,000 \text{ in.}^4 \\ &= 168,506 \text{ kip-in.}\end{aligned}$$

A moment distribution solution leads to $M = 194,793$ kip-in. at the interior supports, and the moments are distributed along the length of the structure as shown in Fig. B1. The support mo-

ments are 1.156 times the fixed end moments, and the 1.156 factor is specific to the span lengths considered.

This is a positive moment, so it produces a bottom fiber tension of:

$$\begin{aligned}f_{cb} &= 194,793 \text{ kip-in.} * 88.534 \text{ in.} / \\ &\quad 32,005,000 \text{ in.}^4 \\ &= +0.539 \text{ ksi}\end{aligned}$$

The residual stress was -0.228 psi (compression), leaving a net bottom fiber tension stress of $+0.311$ psi tension.

As noted earlier, the residual stress should not be assumed to be too precise, but the conclusion remains that there is a significant bottom fiber tension throughout the interior span as a consequence to the thermal loading.

* * *